Estimation of helical angles of myosin and collagen by second harmonic generation imaging microscopy.

François Tiaho, Gaëlle Recher, Denis Rouède

Estimation of helical angles of myosin and collagen by second harmonic generation imaging microscopy

François Tiaho[1], **Gaëlle Recher**[1], **Denis Rouède**[2]

[1]*Equipe SCANING, CNRS UMR 6026, Université de Rennes1, Campus de Beaulieu, 35042 Rennes Cedex, France*

[2]*Equipe Biophysique, CNRS UMR 6626, Institut de Physique de Rennes, Université de Rennes1, Campus de Beaulieu, 35042 Rennes Cedex, France*

denis.rouede@univ-rennes1.fr

Abstract: We performed Second Harmonic Generation (SHG) imaging microscopy of endogeneous myosin-rich and collagen-rich tissues in amphibian and mammals. We determined the relative components of the macroscopic susceptibility tensor $\chi^{(2)}$ from polarization dependence of SHG intensity. The effective orientation angle θ_e of the harmonophores has been determined for each protein. For myosin we found $\theta_e \approx 62^\circ$ and this value was unchanged during myofibrillogenesis. It was also independent of the animal species (xenopus, dog and human). For collagen we found $\theta_e \approx 49^\circ$ for both type I- and type III- rich tissues. From these results we localized the source of SHG along the single helix of both myosin and collagen.

OCIS codes: (180.0180) Microscopy; (190.4160) Multiharmonic generation; (170.0180) Biology and medicine

References and links

1. P. J. Campagnola, A. C. Millard, M. Terasaki, P. E. Hoppe, C. J. Malone and W. A. Mohler, "Three-dimensional high-resolution second-harmonic generation imaging of endogenous structural proteins in biological tissues," Biophys. J. **82,** 493–508 (2002).
2. P. J. Campagnola and L. M. Loew, "Second-harmonic imaging microscopy for visualizing biomolecular arrays in cells, tissues and organisms," Nat. Biotechnol. **21,** 1356–1360 (2003).
3. W. A. Mohler, A. C. Millard and P. J. Campagnola, "Second harmonic generation imaging of endogenous structural proteins," Methods, **29,** 97–109 (2003).
4. I. Freund and L. Kopf, "Long-Range Order in NH4Cl," Phys. Rev. Lett. **24,** 1017–1021 (1970).
5. D. A. Kleinman, "Nonlinear dielectric polarization in optical media," Phys. Rev. **126,** 1977–1979 (1962).
6. T. Boulesteix, E. Beaurepaire, M. P. Sauviat and M. C. Schanne-Klein, "Second-harmonic microscopy of unstained living cardiac myocytes: measurements of sarcomere length with 20-nm accuracy," Opt. Lett. **29,** 2031–2033 (2004).
7. S. V. Plotnikov, A. C. Millard, P. J. Campagnola and W. A. Mohler, "Characterization of the myosin-based source for second-harmonic generation from muscle sarcomeres," Biophys. J. **90,** 328–339 (2006).
8. C. Greenhalgh, N. Prent, C. Green, R. Cisek, A. Major, B. Stewart and V. Barzda, "Influence of semicrystalline order on the second-harmonic generation efficiency in the anisotropic bands of myocytes," Appl. Opt. **46,** 1852–1859 (2007).
9. I. Freund, M. Deutsch and A. Sprecher, "Connective tissue polarity. Optical second-harmonic microscopy, crossed-beam summation, and small-angle scattering in rat-tail tendon," Biophys. J. **50,** 693–712 (1986).
10. S. Roth and I. Freund, "Second harmonic generation in collagen," J. Chem. Phys. **70,** 1637–1643 (1979).
11. K. Beck and B. Brodsky, "Supercoiled protein motifs: the collagen triple-helix and the α-helical coiled coil," J. Struct. Biol. **122,** 17–29 (1998).

#85755 - $15.00 USD Received 26 Jul 2007; revised 27 Aug 2007; accepted 30 Aug 2007; published 12 Sep 2007

12. P. D. Nieuwkoop and J. Faber, *Table of Xenopus laevis (Daudin)*, (Garland Publishing Inc, New York, 1967).
13. M. B. Ferrari and N. C. Spitzer, "Calcium signaling in the developing xenopus myotome," Dev. Biol. **213,** 269–289 (1999).
14. Y. Nakae, P. J. Stoward, T. Kashiyama, M. Shono, A. Akagi, T. Matsuzaki and I. Nonaka, "Early onset of lipofuscin accumulation in dystrophin-deficient skeletal muscles of DMD patients and mdx mice," J. Mol. Histol. **35,** 489–499, (2004).
15. C. Alexakis, T. Partridge and G. Bou-Gharios, "Implication of the satellite cell in dystrophic muscle fibrosis: a self perpetuating mechanism of collagen over-production," Am. J. Physiol. Cell. Physiol. (2007) (to be published).
16. M. Strupler, A. M. Pena and M. Hernest, "Second harmonic imaging and scoring of collagen in fibrotic tissues," Opt. Express **15,** 4054–4065 (2007), http://www.opticsexpress.org/abstract.cfm?id=131626.
17. Y. R. Shen, "Surface properties probed by second-harmonic and sum-frequency generation," Nature **337,** 519–525 (1989).
18. S. W. Chu, S. Y. Chen, G. W. Chern, T. H. Tsai, Y. C. Chen, B. L. Lin and C. K. Sun, "Studies of $\chi^{(2)}/\chi^{(3)}$ tensors in submicron-scaled bio-tissues by polarization harmonics optical microscopy," Biophys. J. **86,** 3914–3922 (2004).
19. R. M. Williams, W. R. Zipfel and W. W. Webb, "Interpreting second-harmonic generation images of collagen I fibrils," Biophys. J. **88,** 1377–1386 (2005).
20. J. F. Nye, *Physical Properties of Crystals*, (Oxford University Press, Oxford, 1985).
21. W. H. Press, B. P. Flannery, S. A. Teukolsky and W. T. Veterlin, *Numerical Recipe* (Section 14.4), (Cambridge, 1986).
22. T. F. Heinz, H. W. K. Tom and Y. R. Shen, "Determination of molecular orientation of monolayer adsorbates by optical second-harmonic generation," Phys. Rev. A **28,** 1883–1885 (1983).
23. P. F. Brevet, *Surface Second Harmonic Generation*, (first edition, Presses Polytechniques et Universitaires Romandes, Lausanne, 1996).
24. A. Leray, L. Leroy, Y. Le Grand, C. Odin, A. Renault, V. Vié, D. Rouède, T. Mallegol, O. Mongin, M. H. V. Werts and M. Blanchard-Desce, "Organization and orientation of amphiphilic push-pull chromophores deposited in Langmuir-Blodgett monolayers studied by second-harmonic generation and atomic force microscopy," Langmuir **20,** 8165–8171 (2004), http://www.perso.univ-rennes1.fr/denis.rouede/research/la0491706.pdf.
25. G. J. Simpson and K. L. Rowlen, "An SHG magic angle: dependence of second harmonic generation orientation measurements on the width of the orientation distribution," J. Am. Chem. Soc. **121,** 2635–2636 (1999).
26. P. Stoller, B. M. Kim, A. M. Rubenchik, K. M. Reiser and L. B. Da Silva, "Polarization-dependent optical second-harmonic imaging of a rat-tail tendon," J. Biomed. Opt. **7,** 205–214 (2002).
27. J. Bella, M. Eaton, B. Brodsky and H. M. Berman, " Crystal and molecular structure of a collagen-like peptide at 1.9 *Å* resolution," Science **266,** 75–81 (1994).

1. Introduction

Second harmonic generation (SHG) imaging microscopy has recently appeared to be a powerful tool to image intrinsic subcellular signals from endogeneous proteins such as microtubule, myosin and collagen in living tissues [1, 2, 3]. SHG is sensitive to harmonophore long-range order and thus is very complementary to X-ray diffraction which reports short-range translational order [4, 5]. A lot of effort has been done in the past few years in order to identify the source of SHG from biological striated muscle tissues. Boulesteix et al. [6] first suggested that the main contribution to the emitted signal could reside in the myosin head whereas Plotnikov et al. [7] showed that SHG is related to the thick filament of the sarcomere. More recently it has been suggested that the motion of myosin heads during contraction affects the semicrystalline order and therefore the intensity of SHG signal [8]. In order to provide more information on the origin of SHG in fibrilar proteins, we investigated in the present work the polarization dependence of SHG intensity generated by thin slices of striated muscles and of collagen-rich tissues from different species (*Xenopus laevis*, dog and human). We determined the ratio of the components of the macroscopic susceptibility $\chi^{(2)}$ tensor for tissues of myosin and collagen using conventional model of SHG in fibrilar proteins [9, 10]. Under the assumption of a dominant hyperpolarizabity coefficient β, an effective orientation angle θ_e of the harmonophores has been deduced. For all myosin-rich tissues, we found that this angle was almost constant with a mean value of about $\theta_e \approx 62^\circ$. This value was independent of (i) the muscle developmental stage for *Xenopus laevis* and (ii) the studied species. In collagen I- and III-rich tissues, we found a

#85755 - $15.00 USD Received 26 Jul 2007; revised 27 Aug 2007; accepted 30 Aug 2007; published 12 Sep 2007

distinct mean angle of about $\theta_e \approx 49°$. These values are close approximations of the helical pitch angle deduced from X-rays structural parameters of helices of both myosin and collagen [11].

2. Experimental methods

2.1. Tissue preparation

Muscle tissues were obtained from tadpole tails (stage 32, 37 and 46) of *Xenopus laevis* [12] animals, gastrocnemius of adult xenopus (national breeding facility of xenopus animals in Rennes, France), gastrocnemius of a four months old Golden retriever dog with Duchenne muscular dystrophy (DMD) (provided by Pr. Y. Cherel, ENV, Nantes, France), gastrocnemius of adult healthy Beagle dog (Biotrial, Rennes, France) and gastrocnemius of 71 years old human female (provided by E . Berton, Department of Pathology, Rennes, France). Collagen-rich tissues were obtained from xenopus tendon and aorta and from epimysium of healthy Beagle dog. Muscles were dissected, fixed over night in PFA 4 % at 4°C, and rinsed at least three times with the appropriate saline buffer. We used either isolated fibers from some adult xenopus or 100 μm-thick slices obtained by slicing horizontally agarose-embedded muscles, glued on the stage of a vibroslicer (LEICA, VT 1200S).

2.2. Imaging system

The setup (PIXEL (http://pixel.univ-rennes1.fr/) platform of EUROPIA, University of Rennes1, France) was based on a Leica TCS SP2 confocal scanning head coupled to a Leica DMIRB inverted microscope with a MAITAI Spectra Physics femtosecond laser. A Leica objective HC-PLAPO 20X (NA=0.7) or an Olympus water immersion objective LUMFL 60X (NA=0.9) were used for applying 10-20 mW of 940 nm excitation at the sample. The SHG signal was collected in a forward direction using either a S23 (NA=0.53) or a multi-immersion S1 (NA=0.90-1.4) Leica condenser. A BG39 bandpass filter and a 470 nm IR filter (10 nm FWHM) were placed before the PMT. The dichroic filter wheel of the microscope was removed and replaced by a computer control PR50CC Newport rotation stage (precision 0.1°) equiped with an achromatic zero-order Quartz-MgF_2 half-wave plate in order to adjust the polarization angle of the incident IR electric field without movement of the biological specimen.

3. Experimental results

To determine the effect of myofibrillogenesis on SHG signal, we have studied xenopus tadpoles swimming muscles from 1 (stage 32), 2 (stage 37) and 4 (stage 46) days post fertilization (dpf). These developmental stages coincide with the intense period (stage 26 to stage 36) of myofibrillogenesis that has been shown to be under the control of intracellular calcium in this species [13]. In Fig. 1, we present SHG forward images from thin specimens of xenopus muscles (Fig. 1(a-d)). All the specimens were positionned on the fixed stage of the microscope (YZ plane) of the laboratory coordinate systems (X, Y, Z) with light propagating in the X direction (see the inset of Fig. 1(a)). At embryonic stage 32 (1 dpf) muscle fibers have not fully developed their sarcomeres as indicated by large regions of cells without SHG signal (Fig. 1(a)), and the average myocyte diameter was about 15 μm. At stage 37 (Fig. 1(b)) full development of sarcomers was achieved. At this stage, corresponding also to hatching, no significant modification of the diameter of the myocyte was observed. At 4 dpf, *in vivo* SHG images reported a significant growth of the myocytes with an average measured diameter of 25 μm (Fig. 1(c)). Overall SHG images from body wall swimming muscles at these developmental stages revealed an increase in the number of sarcomeres and in the size of the striated myocytes. During the developmental stages 32 to 46, this growth is in relation with the size of the animal which in-

#85755 - $15.00 USD Received 26 Jul 2007; revised 27 Aug 2007; accepted 30 Aug 2007; published 12 Sep 2007

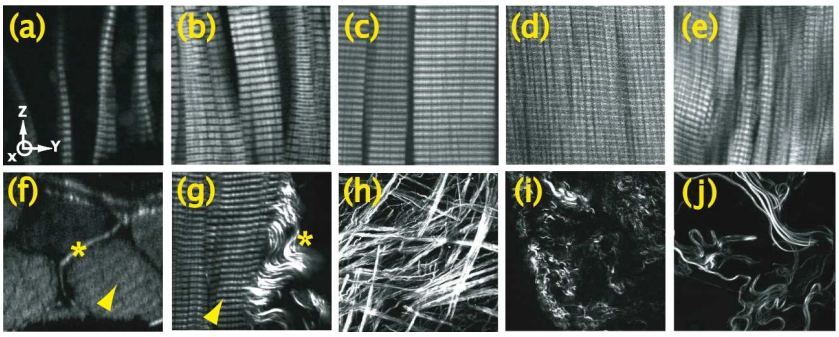

Fig. 1. Optical sections illustrating SHG images from different muscles and collagen-rich tissues. (a-c): swimming body muscles of developing xenopus tadpoles of respectively 1 day (stage 32), 2 days (stage 37) and 4 days (stage 46) post fertilization. (d): gastrocnemius muscle of adult xenopus. (e): gastrocnemius muscle of a 71 years old human female. (f,g): gastrocnemius muscle and collagen of 4 months old Golden retriever dog with DMD. (h-j): collagen from respectively adult xenopus tendon and aorta and adult healthy Beagle dog muscle. Images (a-e, g) are optical section images of $50\times50\mu m^2$ while image (f) is a $90\times90\mu m^2$ XY crossed-section. Note the presence of ectopic collagen in the endomysium (star). Arrowhead indicated a transsected muscle fiber. (g): Arrowhead and star indicated respectively muscle and ectopic collagen fibers. (h): Projection of $100\mu m$ thick stack of a $500x500\mu m^2$ image. (i,j): Projection of $17\mu m$ thick stack of a $500x500\mu m^2$ image. Note that image (c) was obtained from *in vivo* 46 stage xenopus larva and image (j) was obtained from fresh slice of Beagle dog muscle whereas all other images were from PFA-fixed tissues.

creases from 5 mm at stage 32 (1dpf) to 10 mm at stage 46 (4 dpf). For adult xenopus we have chosen the gastrocnemius muscle that is also implicated in locomotion since the swimming tail muscles are lost during metamorphosis of the tadpole at stage 66 (58 dpf). Adult gastrocnemius muscle of xenopus was characterized by bundles of muscle fibers emitting SHG signal whose fibers form a syncytium (with average size 150 μm) in which individual myocyte could not be distinguished (Fig. 1(d)). This syncytial organization of muscle fibers deduced from SHG images was also seen with the gastrocnemius muscles of adult human (Fig. 1(e)) and with a four months old Golden retriever dog with Duchenne muscular dystrophy (DMD) (Fig. 1(f,g)). DMD is a muscle pathology related to a defect of the dystrophin gene with a great reduction of the cytoskeletal dystrophin protein that ultimately leads to portion or total muscle fibers degeneration [14] and appearance of ectopic collagen (probably type I) in the endomysium (collagen IV rich tissue wrapping each musle fiber) [15]. The average size of bundles were 68 μm and 41 μm respectively for human and dog. Concerning Golden retriever with DMD, it was easy to find a field of view with SHG emission from both muscle myosin and supposed extracellular matrix as illustrated in Fig. 1(f, g). The collected signal from myosin was characterized by its striated sarcomeric organization whereas the one from the extracellular matrix was more intense and had a fibrous shape. In order to better characterize the difference between the two SHG signals, collagen-riched tissues like adult xenopus tendon or aorta and adult healthy Beagle dog fresh epimysium (probably type III) (Fig. 1(h-j)) were chosen. According to tissue distribution, we expected type I collagen in tendon, type III in aorta and in epimysium (conjonctive tissue wrapping bundle of muscle fibers). In this later case a fresh specimen was used to probe any artifact that could result from the PFA fixing protocol. Type IV collagen is also expected in muscle endomysium but has been shown to lack SHG signal [16] and therefore could not

#85755 - $15.00 USD Received 26 Jul 2007; revised 27 Aug 2007; accepted 30 Aug 2007; published 12 Sep 2007

explain the observed signal in Fig. 1(f,g).

Next we compared the polarization dependence of SHG signal from different striated muscles (Fig. 2) to that of collagen-rich tissues (Fig. 3) with the aim of finding a signature of each type of endogeneous harmonophore. A sufficient image enlargment was used to cautiously align the myosin and collagen filaments along axis Z of the laboratory coordinates (X, Y, Z) such that the average misalignment was less than 5°. As an example, images for adult gastrocnemius muscle and tendon are shown respectively in Fig. 2(a) and Fig. 3(a) for different values of the polarization angle α of the incident IR electric field. For each studied specimen, we performed a serie of images with 10° step rotation of angle α. The images were quantitatively analyzed with open source ImageJ software http://rsb.info.nih.gov/ij/ and mean SHG intensity of a particular ROI in each serie was drawn as a function of α (see Fig. 2(b)) (no polarizer was placed between the sample and the detection PMT). For each specimen, the same polarization curve was identically reproduced for different ROIs. The experimental data were analytically fitted with KaleidaGraph 3.6 (Synergy Software) using Equation 2 according to the theoretical model described in next section and we obtained the best fit of the experimental data when the average misalignment within a ROI was less than 5°. In sub-ROIs where misalignments of the fibrils along axis Z were greater than 5°, angular correction was necessary in the simulation to fit the data with the same identical adjustable parameters. Concerning experimental results, one

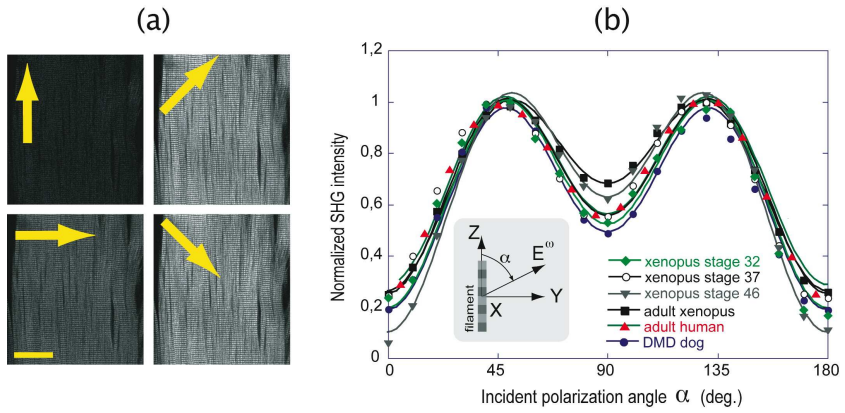

Fig. 2. Polarization dependence of the SHG signal of different muscles. (a): SHG optical sections of adult xenopus gastrocnemius muscle illustrating the effect of four different incident polarization angles α (0°, 45°, 90°, 135°) on the emitted signal from the same field of view. Scale bar: 20 μm. Arrows represent the polarization of the incident electric field (0 degree is vertical). (b): normalized SHG signal as a function of the incident polarization angle α for different muscles of different species. Experimental data are represented with different symbols. ♦, ○ and ▼ from xenopus tadpole body wall muscles of respectively 1 day (stage 32), 2 days (stage 37) and 4 days (stage 46). ■, ▲ and ● from adult gastrocnemius muscles of respectively xenopus, 71 years old human female and DMD Golden retriever dog. The full lines are drawn using the best fit obtained from Eq. 2. On the inset, a schematic top view is shown. The long axis of myosin filaments for each specimen was oriented along the Z axis of the laboratory coordinates (X, Y, Z).

should note that (see Fig. 2(b)) the maximum SHG intensity does not occur with the incident electric field being parallel to the myosin filament but instead for an angle which is almost identical and equal to 50° and 130° for all specimens. The minimum intensity is obtained when the incident polarization is exactly parallel to the axis of the fiber. Note that *in vivo* stage 46 tad-

#85755 - $15.00 USD Received 26 Jul 2007; revised 27 Aug 2007; accepted 30 Aug 2007; published 12 Sep 2007

pole presented the lowest normalized SHG intensity suggesting a slight difference in the signal properties between fresh and PFA-fixed muscle tissues. The curve describing the myosin SHG signal of DMD dog is similar to that obtained with healthy muscles from xenopus and human suggesting that the intact non-degenerated portion of fibers retained all the required properties for SHG emission. Overall the polarization dependence SHG signal signature from all muscle tissues was conserved and was independent of (i) the developmental stage and (ii) the animal species. The same study was performed in collagen-rich tissues and the corresponding polarization dependence of SHG intensity is shown in Fig. 3(b). The angular dependence of the SHG intensity is rather different in that case since the minimum intensity is obtained when the incident polarization is exactly perpendicular to the axis of the fiber. For collagen-rich tissues a conserved SHG signature different from myosin was observed without any difference between the fresh epimisium and the other PFA-fixed specimens. Moreover one should notice that the greatest difference in SHG signal occurs at $\alpha = 0$ with ≈20% and ≈80% of peak intensity for respectively myosin and collagen.

In next section we develop an appropriate model in order to quantitatively characterized the polarization dependence of SHG intensity of myosin- and collagen-rich tissues and to gain insight into the molecular orientation and organization of the harmonophores.

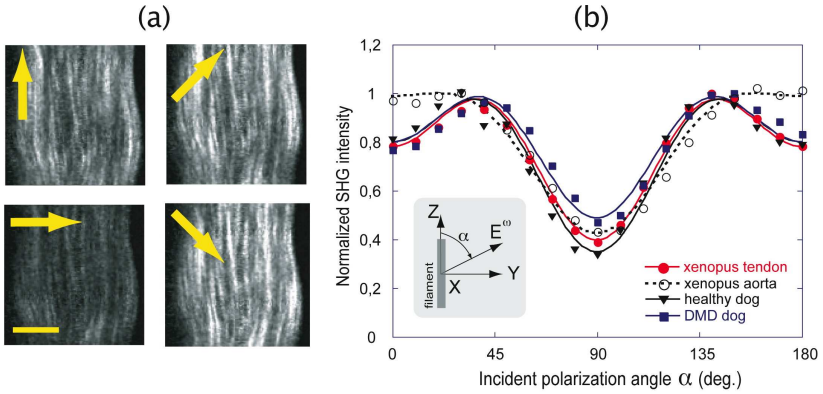

Fig. 3. Polarization dependence of the SHG signal of different collagen-rich tissues. (a): SHG optical sections of adult xenopus tendon illustrating the effect of four different incident polarization angles α (0°, 45°, 90°, 135°) on the emitted signal from the same field of view. Scale bar: 10 μm. Arrows represent the incident polarization angles α. (b): normalized SHG signal as a function of the incident polarization angle α for different collagen-rich tissues of xenopus and dog. Experimental data are represented with different symbols. ●, ○ respectively for xenopus tendon and aorta. ▼ and ■ respectively for epimysium of healthy dog and muscles of DMD dog. Note that data from healthy dog muscle epimysium was from fresh slice whereas all other data were from PFA-fixed tissues. The lines are drawn from the best fit obtained from Eq. 2. On the inset, a schematic top view is shown. The long axis of collagen filaments for each specimen was oriented along the Z axis of the laboratory coordinates (X, Y, Z).

4. Theoretical analysis

As a rule, second harmonic electric fields $E^{2\omega}$ at 2ω originate from nonlinear polarization $P^{2\omega} = \chi^{(2)} E^{\omega} E^{\omega}$ by mixing of intense electric fields E^{ω} at ω in the medium [17]. $\chi^{(2)}$ is the macroscopic nonlinear susceptibility tensor and assuming that the distribution of myosin and collagen undergoes cylindrical symmetry [7, 9, 10, 18, 19] along the main axis Z of the filament,

#85755 - $15.00 USD Received 26 Jul 2007; revised 27 Aug 2007; accepted 30 Aug 2007; published 12 Sep 2007

the only nonvanishing components of $\chi^{(2)}$, described by a C_6 tensor, reduces to $\chi^{(2)}_{ZZZ}$(=χ_{33}), $\chi^{(2)}_{iiZ}$=$\chi^{(2)}_{iZi}$(=χ_{15}) and $\chi^{(2)}_{Zii}$ (=χ_{31}) for i=X or Y in the laboratory coordinates (X, Y, Z) [20]. Considering that light is propagating along direction X, one obtains the following equation in the tranverse wave approximation ($E^{\omega}_X = 0$)

$$\begin{aligned} P^{2\omega}_X &= 0 \\ P^{2\omega}_Y &= 2\chi_{15} E^{\omega}_Y E^{\omega}_Z \\ P^{2\omega}_Z &= \chi_{31}(E^{\omega}_Y)^2 + \chi_{33}(E^{\omega}_Z)^2. \end{aligned} \tag{1}$$

The SHG intensity $I^{2\omega} \sim [(P^{2\omega}_Y)^2 + (P^{2\omega}_Z)^2]$ can be derived from Eq. 1 using $E^{\omega}_Y = \sin\alpha$ and $E^{\omega}_Z = \cos\alpha$ so as to obtain the standard polarization dependence of SHG intensity for polar filaments [9, 18]

$$I^{2\omega} \sim [\sin^2 2\alpha + (\frac{\chi_{31}}{\chi_{15}}\sin^2\alpha + \frac{\chi_{33}}{\chi_{15}}\cos^2\alpha)^2]. \tag{2}$$

We have used a nonlinear least-squares fit with the Levenberg-Marquardt method [21] in order to adjust the fitting parameters χ_{31}/χ_{15} and χ_{33}/χ_{15} with the experimental data of Fig. 2(b) and Fig. 3(b) and the values of these parameters for both myosin and collagen are reported in Table 1. One should notice that χ_{31}/χ_{15} is close to unity fo all myosin- and collagen-rich

Table 1. Ratio of coefficients χ_{31}/χ_{15} and χ_{33}/χ_{15} for myosin-rich and collagen-rich tissues obtained from fit of Eq. 2 with the experimental data of Fig. 2(b) and Fig. 3(b). The orientation parameter D and the effective orientation angle θ_e are defined by Eq. 4.

	χ_{31}/χ_{15}	χ_{33}/χ_{15}	D	$\theta_e(deg)$
myosin of stage 32 xenopus	0.89	0.55	0.21	62.3
myosin of stage 37 xenopus	0.95	0.64	0.24	60.5
myosin of stage 46 xenopus	0.95	0.38	0.16	66.4
myosin of adult xenopus	1.12	0.70	0.26	59.4
myosin of DMD Golden retriever dog	0.87	0.54	0.21	62.5
myosin of 71 years old human female	0.97	0.69	0.25	59.6
collagen of adult xenopus tendon	1.02	1.44	0.41	50.3
collagen of adult xenopus aorta	1.41	2.15	0.52	43,9
collagen of DMD Golden retriever dog	1.21	1.56	0.44	48.5
collagen of healthy Beagle dog	0.94	1.43	0.41	49.7

tissues while the mean ratio of χ_{33}/χ_{15} was found to increase from ≈0.6 for myosin to ≈1.5 for collagen. In order to deduce the microscopic parameters, $\chi^{(2)}$ has to be related to the hyperpolarizability tensor $\beta^{(2)}$ of the nonlinear molecules. Under the assumption of a cylindrical distribution of harmonophores, the derivation is similar to the one developed for monolayers of deposited chromophores and in the case of a dominant axial coefficient β, the coherent summation of the individual harmonophores leads to [17, 22, 23, 24]

$$\begin{aligned} \chi_{33} &= N_s\beta < \cos^3\theta > \\ \chi_{15} = \chi_{31} &= \frac{1}{2}N_s\beta < \cos\theta\sin^2\theta > . \end{aligned} \tag{3}$$

In this equation, θ is the polar angle of the nonlinear molecule with axis Z, N_s is the number density of active harmonophores and the brackets $<>$ indicates an orientational average over the distribution of molecular orientation. It is useful to notice that Eq. 3 assumes χ_{15}=χ_{31} and

#85755 - $15.00 USD Received 26 Jul 2007; revised 27 Aug 2007; accepted 30 Aug 2007; published 12 Sep 2007

as this equality is verified for almost all of our results, the assumption of a dominant hyperpolarizability coefficient β seems reasonable for both myosin and collagen tissues. Under this assumption, the meaningful orientation parameter D can also be defined from Eq. 3 [24, 25]

$$D = \frac{<\cos^3\theta>}{<\cos\theta>} = \frac{\chi_{33}/\chi_{15}}{2+\chi_{33}/\chi_{15}} = \cos^2\theta_e\,. \tag{4}$$

D was initially introduced to describe orientation and disorder of molecules at surfaces and interfaces. Regarding θ_e, this angle was defined in reference [24] as an effective (or apparent) angle corresponding to the most probable orientation of the active molecules when the distribution of molecular orientation is very narrow [24, 25]. These parameters can be used here to evaluate the organization of the harmonophores in myosin- and collagen-rich tissues. The values of D and θ_e derived from Eq. 4 are thus reported in Table 1 and one should notice a weak dispersion of the data around mean values $D \approx 0.22$, $\theta_e \approx 62^\circ$ and $D \approx 0.42$, $\theta_e \approx 49^\circ$ for respectively myosin-rich and collagen-rich tissues (the result for xenopus aorta was not taken into account since in that case the approximation χ_{31}/χ_{15} close to unity was not fullfilled). The difference in the values of D obtained for the two proteins underlines a distinct harmonophore organization as it will be discussed in the following.

5. Discussion

Polarization dependence of SHG intensity for myosin from *in vivo* or PFA-fixed tissues, from different developmental stages in xenopus and from different animal species (xenopus, dog and human) has revealed the same angular signature with a conserved value of the effective harmonophore orientation angle θ_e. This signature, which was observed from intact non-degenerated portion of DMD muscle fibers was found to be different to that of ectopic collagen that appeared in the endomysium of this pathological muscle suggesting that SHG polarization is an efficient method to distinguish between myosin and collagen. Extension of SHG study to different types (I and III) collagen-rich tissues from fresh or PFA-fixed tissues also revealed a conserved signature of this fibrillar protein with a different harmonophore orientation angle θ_e. Previous polarization studies of SHG intensity, from mouse either leg muscles [18] or myofibrils of scallops adductor [7], from rat-tail tendon [9, 10, 26] and from mouse-leg tendon [7], concerning the values of either $\chi^{(2)}$ coefficients or θ_e, are in good agreement with our measurements. We showed that under the approximation of a dominant hyperpolarizability coefficient β with a cylindrical distribution of harmonophores, most of our experimental results could be fitted using standard model of SHG. Our extended SHG intensity study from myosin- and collagen- riched tissues suggests that the apparent orientation angles of the harmonophores are conserved for each protein and are close approximation of the angles of each helix relative to the main filament axis as obtained by X-rays diffraction [11, 27]. The single helices parameters (helix pitch P and radius R) are given in references [11, 27] for myosin (P=5.5$\AA$, R=2.2$\AA$) and collagen (P=9.5$\AA$, R=1.5$\AA$). Using $\tan\theta = 2\pi R/P$, the respective pitch angles $\theta = 68^\circ$ and $\theta = 45^\circ$ for myosin and collagen can be deduced which values are close to our data.

Mean values of the orientation parameter $D \approx 0.22$ and $D \approx 0.42$ for respectively myosin-rich and collagen-rich tissues were obtained within the analyzed ROIs. For each analyzed specimen, the error on D value was about 5% and this precision was achieved for analyzed ROIs where the average fibril misalignment was less than 5°. The misalignment of fibrils ($>5^\circ$) in sub-ROIs can be corrected during simulation to fullfill the approximation $\chi_{15}=\chi_{31}$ and therefore to yield the same value of D. Overall, the value of D is independent of the angular orientation of the fibers. For each protein, we obtained a dispersion of the value of D less than 25% for all studied specimens which is far less than the 200% variation between the D values of the two proteins. Therefore, the value of D can be considered as an intrinsic property of each protein and the

#85755 - $15.00 USD Received 26 Jul 2007; revised 27 Aug 2007; accepted 30 Aug 2007; published 12 Sep 2007

difference could reflect a different state of orientational disorder. Indeed, it is clear from Eq. 4 that the effective angle θ_e merges into the angle of maximum probability θ_o as the distribution function of molecular orientation sharpens. Otherwise, the maximum discrepancy between θ_e and θ_o depends on the value of D and on the magnitude of harmonophore orientational disorder [24]. In order to take into account this disorder, the average in Eq. 4 has to be performed and the distribution function has to be specified. We can use the results of reference [24] to evaluate the possible expanse of this orientational disorder. In this work, it was shown that the use of a uniform distribution of molecular orientation could account for most of the significant results. This distribution is defined for equal probability of orientation angles around a mean value θ_o and has a full width δ of angular disorder. Using this distribution, the average in Eq. 4 can be performed and a simple analytical relation can be derived [24]

$$D(\delta,\theta_o) = \frac{1}{2}\,(1+\cos\delta\cos 2\theta_o). \tag{5}$$

This equation clearly shows that different values of θ_o and δ, representing a different situation of orientational disorder, can give the same value of D. Moreover, for any value of δ, θ_e always underestimates θ_o ($\cos 2\theta_e = \cos\delta\cos 2\theta_o$). Equation 5 was defined for an angular variation limited to $[0\ \pi/2]$ what corresponds in our case to a fully stretched (θ_o=0°) or compressed (θ_o=90°) helix. The graphical solution of Eq. 5 showing all possible values of θ_o and δ for fixed value of D is given in Fig. 9 of reference [24] but it is easy to verify that mean orientation angle θ_o is ranging from 62° to 69° for myosin (D ≈ 0.22) and 49° to 57° for collagen (D ≈ 0.42) according to the limited angular interval chosen [0, π/2]. The associated disorder is ranging from δ=0° to δ=41° for myosin and δ=0° to δ=67° for collagen. A schematic view of single helix of both myosin and collagen showing mean angle θ_o and maximum possible angular disorder δ is given in Fig. 4. It is of interest to notice that the mean value of D ≈ 0.42 found for collagen is

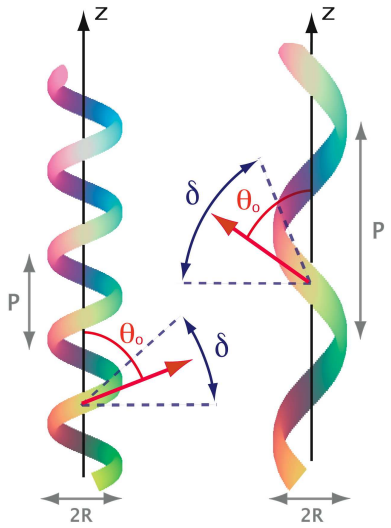

Fig. 4. Schematic view of single helix of myosin (left) and collagen (right). Mean harmonophore orientation angle θ_o and disorder width δ are shown. According to the model, θ_o is ranging from 62° to 69° for myosin and 49° to 57° for collagen with maximum disorder width δ=41° (D=0.22, θ_o=69°) for myosin and δ=67° (D=0.42, θ_o=57°) for collagen. P and R are helix pitch and radius. For myosin P=5.5Å, R=2.2Å and for collagen P=9.5Å, R=1.5Å [11, 27].

#85755 - $15.00 USD Received 26 Jul 2007; revised 27 Aug 2007; accepted 30 Aug 2007; published 12 Sep 2007

close to the limit value of 0.5 (θ_e=45°) which allows maximum possible disorder δ=90° within the model. This possible disorder could originate from the superhelical structure of the two fibrillar proteins. Superhelical assembly requires stabilization forces, and the number and the type of interactions between chains of myosin and collagen superstructures are different [11]. In the case of collagen triple helix, stabilization is mainly due to hydrogen bonding and there is only one bond per (Gly-X-Y) triplet. Concerning myosin, the interactions between chains are more numerous and more cohesive since there is one hydrogen bond per amino-acid (corresponding to three times more than in collagen). Moreover, the assembly of myosin superhelix is "locked" by hydrophobic and electrostatic interactions. Taken together, these observations suggest that collagen seems to be more flexible than myosin and this reinforces the possibility to have more orientational disorder for this protein.

6. Conclusion

In this report we show from extensive studies performed on amphibian and mammals that myosin and collagen are efficiently discriminated by different signatures of polarization dependence of SHG signal. The deduced orientation angles of harmonophores in myosin-rich and collagen-rich tissues, using conventional model of SHG in fibrillar proteins, match the pitch angles of the single helices of these two proteins. Overall the polarization dependence study of SHG signal appears to be a non-invasive and efficient method for probing molecular organization of endogeneous fibrillar proteins and could be a valuable tool to diagnose diseases involving either myosin or collagen structural disorders.

Acknowledgments

We thanks Région Bretagne, Rennes Métropole, Conseil Général d′Ille-et-Villaine for their financial support and Hélène Mereau, Florence Billon, Amandine Rojo for their technical help.

#85755 - $15.00 USD Received 26 Jul 2007; revised 27 Aug 2007; accepted 30 Aug 2007; published 12 Sep 2007